

Structures, Thermal Stability, and Chemical Activity of Crown-Jewel-Structured Pd–Pt Nanoalloys

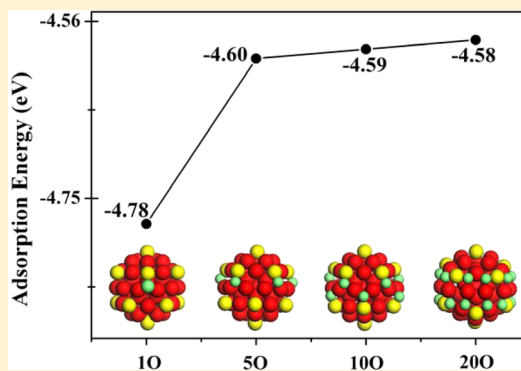
Yang Yang,[†] Zheng Zhao,[†] Rong Cui,[‡] Hao Wu,[‡] and Daojian Cheng*,^{†,‡}

[†]State Key Laboratory of Organic–Inorganic Composites, Beijing University of Chemical Technology, Beijing 100029, People's Republic of China

[‡]Changzhou Institute of Advanced Materials, Beijing University of Chemical Technology, Changzhou 213164, People's Republic of China

Supporting Information

ABSTRACT: In this work, the equilibrium structures, thermal stability, and chemical activity of crown-jewel (CJ)-structured Pd–Pt nanoalloys with highly symmetric cuboctahedral (Cubo), decahedral (Dec), and icosahedral (Ico) structures are studied by using molecular simulation based on the Gupta empirical potential and density functional theory (DFT) calculations. It is found that both the melting temperature and stability of CJ-structured Pd–Pt nanoalloys with the same size follow the order of Ico > Dec > Cubo, which agrees with the rule that the more stable the cluster, the higher the melting point. In addition, the melting temperature of CJ-structured Pd–Pt nanoalloys with the same morphology is of the same linear behavior with the inverse diameter of the clusters, which is consistent with the Pawlow's law. The adsorption properties of O on these Pd–Pt nanoalloys are studied to model the chemical activity of these nanoalloys. For the CJ-structured $Pd_{12}Pt_{43}$, the adsorption strength of O follows the order of Dec < Cubo < Ico, and the adsorption strength per O atom decreases slightly with increasing coverage of the O atom. In addition, the adsorption strength of O on the CJ-structured $Pd_{12}Pt_{43}$ is stronger than that on the CJ-structured $Pd_{12}Pt_{135}$. Our results show that the structures, thermal stability, and chemical activity of CJ-structured Pd–Pt nanoalloys are size- and morphology-dependent, which would shed new light on the design of CJ-structured nanoalloys as catalysts.



1. INTRODUCTION

Bimetallic clusters (or “nanoalloys”) occupy a very important place among nano-objects because they are the building blocks of nanoscience. The rich diversity of compositions, structures, and properties of nanoalloys has led to their widespread applications in catalysis.¹ To achieve a high catalytic activity, special structures of nanoalloys have been found and studied,² such as the core–shell,^{3–5} onion-like,^{6–9} and crown-jewel (CJ)^{10,11} structures. In particular, the CJ structure, where one kind of metal atom (single atom) is controllably assembled at the special position on the surface of the nanoalloys, has been considered to be promising for the catalytic applications. For example, Au–Pd nanoalloys with CJ structure,^{10,11} where the Pd clusters serve as the crowns and the Au atoms serve as jewels decorating the top position of the Pd clusters, were prepared based on the galvanic replacement process, showing excellent catalytic activity for aerobic glucose oxidation. It is obvious that nanoalloys with the CJ structure are worth studying deeply as a potential catalyst. However, data is still scarce for the CJ-structured nanoalloys.

Pt-based nanoalloys have been considered to be promising catalysts for fuel cell cathodes. It is well-known that Pt-based nanoalloys can reduce the utilization of Pt and also improve the

catalytic ability.^{12–15} Among these systems, Pd–Pt nanoalloys have been widely studied, showing enhanced catalytic activity toward the oxygen reduction reaction (ORR).^{16,17} For example, Lim et al.¹⁷ found that Pd–Pt nanoalloys are 2.5 times more active than the Pt/C catalyst for the ORR. Zhang et al.¹⁸ found that the ORR activity on carbon-supported Pd–Pt nanoalloys is 5–8 times higher than that on carbon-supported pure Pt catalyst. It is well-known that structural models can strongly affect not only the thermodynamics but also the catalytic activity and selectivity of metal clusters.¹⁹ In our previous work, $Pd_{43}Pt_{12}$ with a three-shell onion-like structure exhibits the highest relative stability, the highest melting point, and good catalytic activities toward the ORR among these 55-atom Pd–Pt clusters.²⁰ Therefore, it is also interesting to study Pd–Pt nanoalloys with the CJ structure, which could be a promising ORR electrocatalyst. However, little work has been done on the

Special Issue: Current Trends in Clusters and Nanoparticles Conference

Received: October 24, 2014

Revised: December 3, 2014

Published: December 10, 2014

detailed structural properties, melting behaviors, and ORR activity of the CJ-structured Pd–Pt nanoalloys.

Theoretical calculations and simulations have been widely employed to study the detailed structures, thermal stability, and chemical activity of nanoalloys.^{1,21–23} In general, the equilibrium structures and thermal stability of nanoalloys can be explored by using Monte Carlo and molecular dynamics simulations, respectively. In our previous work, the structural stability and melting properties of CJ-structured Au–Pd nanoalloys with the size of 561–2057 atoms were investigated by molecular dynamics simulations.¹¹ It is found that doping of Au atoms on the Pd clusters can decrease the thermal stability of the Pd cluster. It is generally believed that the binding of O is considered as the descriptor of the ORR activity, where the weak O binding strength facilitates the ORR. Therefore, the chemical activity of these Pd–Pt nanoalloys can be modeled based on the adsorption properties of O on these nanoalloys by using density functional theory (DFT) calculations.

In this work, the equilibrium structures, thermal stability, and chemical activity of CJ-structured Pd–Pt nanoalloys are studied by using molecular simulation based on the Gupta empirical potential and DFT calculations. The equilibrium structures of CJ-structured Pd–Pt nanoalloys with the size of 55–561 atoms are obtained by Monte Carlo simulation first, then the melting properties of these nanoalloys are studied by molecular dynamics simulations, and finally the adsorption properties of O on the Pd–Pt nanoalloys with sizes of 55 and 147 atoms are studied by using DFT calculations. For the melting of the CJ-structured Pd–Pt nanoalloys, the effects of the morphology and size are discussed. For the adsorption of O on the CJ-structured Pd–Pt nanoalloys, the effects of the morphology, size, and coverage of O atoms are discussed. The paper is structured as follows. In the next section, we present the computational methodology. Section 3 describes our results and discussion, and section 4 offers our conclusions.

2. CALCULATION DETAILS

2.1. Molecular Simulation. The interaction between metal atoms was modeled semiempirically based on the well-established Gupta potential.^{24,25} It is noted that the Gupta potential has been successfully used to model the structures of elemental metal clusters and nanoalloys effectively.^{26–28} In the Gupta potential, the metal–metal (M–M) interaction energy, $E_{\text{M–M}}$, is given by

$$E_{\text{M–M}} = \sum_i E_{\text{R}}^i + E_{\text{B}}^i \quad (1)$$

where E_{R}^i and E_{B}^i are the Born–Mayer ion–ion repulsion and band interactions, respectively. These two terms for an atom i can be represented based on

$$E_{\text{R}}^i = \sum_{j \neq i} A e^{-p(r_{ij}/r_0 - 1)} \quad (2)$$

$$E_{\text{B}}^i = -\left\{ \sum_j \xi^2 e^{-2q(r_{ij}/r_0 - 1)} \right\} \quad (3)$$

where r_{ij} is the distance between atoms i and j in the cluster, r_0 is the nearest-neighbor distance in the pure metals, and N is the number of the metal atoms. The parameters A , r_0 , ξ , p , and q for the Pd–Pt nanoalloys used in this study are taken from the literature,²⁹ as listed in Table 1. The validity of the Gupta approach for Pd–Pt nanoalloys has been discussed in the

Table 1. Parameters of the Gupta Potential Used in This Work

parameters	Pd–Pd	Pt–Pt	Pd–Pt
A (eV)	0.1746	0.2975	0.23
ξ (eV)	1.718	2.695	2.20
p	10.867	10.612	10.74
q	3.742	4.004	3.87
r_0 (Å)	2.7485	2.7747	2.76

previous work,^{29,30} indicating that the Gupta potential is suitable for describing the Pd–Pt nanoalloys.

In this work, Pd–Pt nanoalloys with highly symmetric cuboctahedral (Cubo), decahedral (Dec), and icosahedral (Ico) structures were studied. To consider the size effect, the nanoalloys with sizes of 55, 147, 309, and 561 were used. For Pd–Pt nanoalloys, only one composition with the fixed 12 Pd atoms was adopted. The semigrand-canonical ensemble Monte Carlo (SEMI-GCMC) simulation was used to obtain the equilibrium structures of the nanoalloys. This method is well-documented in the previous work²² and is found to be effective to obtain the equilibrium structures of nanoalloys.⁹ When this method is used to study the nanoalloys, two trials are introduced in the sampling scheme, (1) random displacement of each atom from its original position and (2) random interchange of two atoms with different species in the cluster.

Molecular dynamics (MD) simulations were performed to study the melting of the Pd–Pt nanoalloys. In this work, MD simulations were carried on using DL_POLY software with a constant number of atoms N with a nearly zero fluctuating pressure P . The temperature was maintained by the Nose–Hoover thermostat. Newton's equations of motion were integrated using the Verlet leapfrog algorithm, and the integration time step was set to 1 fs. For the melting of the nanoalloys, simulations were performed in a series of temperatures starting from 0 to 1200 K with a temperature increment of 50 K. The increment near the melting point was reduced to 10 K. At each temperature, the first 100 ps were used for the atomic structure equilibration, and the next 100 ps were used for the statistical averaging. It is noticed that the degree of accuracy for the obtained melting point can be improved by averaging the melting point on several of the same simulations because the melting range is broader for the medium-sized metal clusters.^{31–33}

2.2. DFT Calculations. DFT calculations were performed using the Quantum Espresso package,³⁴ which is based on a plane wave basis set. The Perdew–Burke–Ernzerhof (PBE) exchange–correlation (xc) functional³⁵ and ultrasoft pseudo-potentials³⁶ were used. Spin-polarized calculations were performed using values of 40 and 320 Ry as the energy cutoff for the description of the wave function and the electronic density for 55-atom nanoalloys, and 30 and 300 Ry were used for 147-atom nanoalloys. The first Brillouin zone was sampled at the Γ point, and the electronic levels were broadened³⁷ with a Gaussian smearing of about 0.002 Ry. The nanoalloy was located in a $30 \times 30 \times 30$ Å cubic supercell for 55-atom nanoalloys and in a $40 \times 40 \times 40$ Å cubic supercell for 147-atom nanoalloys. The positions of the atoms in the complex were fully optimized until the forces were smaller than 0.01 eV/Å per atom.

3. RESULTS AND DISCUSSION

3.1. Equilibrium Configurations. The equilibrium structures of Pd–Pt nanoalloys with highly symmetric Cubo, Dec, and Ico structures were obtained by the SEMI-GCMC simulations. Figure 1 shows the equilibrium structures of CJ-

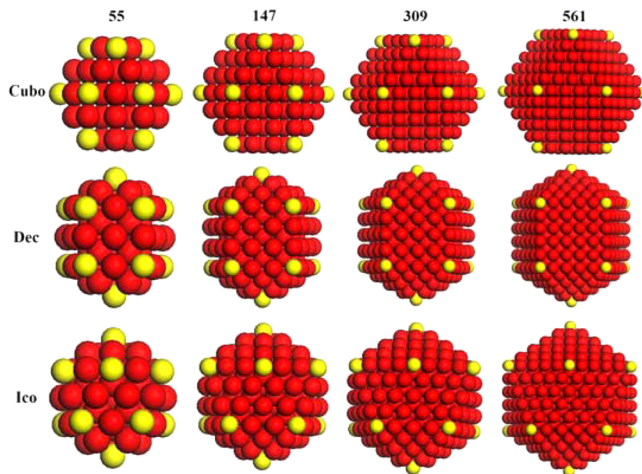


Figure 1. Equilibrium structures of the CJ-structured Pd–Pt nanoalloys with the fixed 12 Pd atoms on the top position changing with the different cluster sizes (55, 147, 309, and 561) and morphologies (Cubo, Dec and Ico).

structured Pd–Pt nanoalloys with the fixed 12 Pd atoms on the top position changing with the different cluster sizes (55, 147, 309, and 561) and morphologies (Cubo, Dec and Ico). For these Pd–Pt nanoalloys, all vertices of the cluster are occupied by 12 Pd atoms, corresponding to the typical CJ structure, where the Pd clusters serve as the crowns and the Pt atoms serve as jewels decorating the top position of the crowns.

To analyze the relative stability of CJ-structured Pd–Pt nanoalloys with different morphologies (Cubo, Dec, and Ico), the total energy per atom was calculated to represent the relative stability of the clusters. Note that the lower the total energy per atom, the more stable the structure of the cluster. Figure 2 shows the total energy per atom of CJ-structured Pd–Pt nanoalloys changing with the different cluster sizes (55, 147, 309, and 561) and morphologies (Cubo, Dec, and Ico). It is found that the values of the total energy per atom of these nanoalloys with the same size follow the order of Ico < Dec < Cubo. It means that the stability of CJ-structured Pd–Pt nanoalloys with the same size follows the order of Ico > Dec > Cubo. Notably, although the Ico is found to be more stable than the Dec and Cubo in this work, the truncated octahedra and Marks Dec are even much more stable than the Ico in some cases.^{38,39}

3.2. Thermal Stability. The parameters such as potential energy and heat capacity can be explored to identify the first-order transition from the solid to liquid phase upon heating.^{30,40–43} In this work, we identify the melting of CJ-structured Pd–Pt nanoalloys by using the caloric curve and the corresponding heat capacity C_v per atom, which is defined by

$$C_v = \frac{(\langle E^2 \rangle - \langle E \rangle^2)}{nk_B T^2} \quad (4)$$

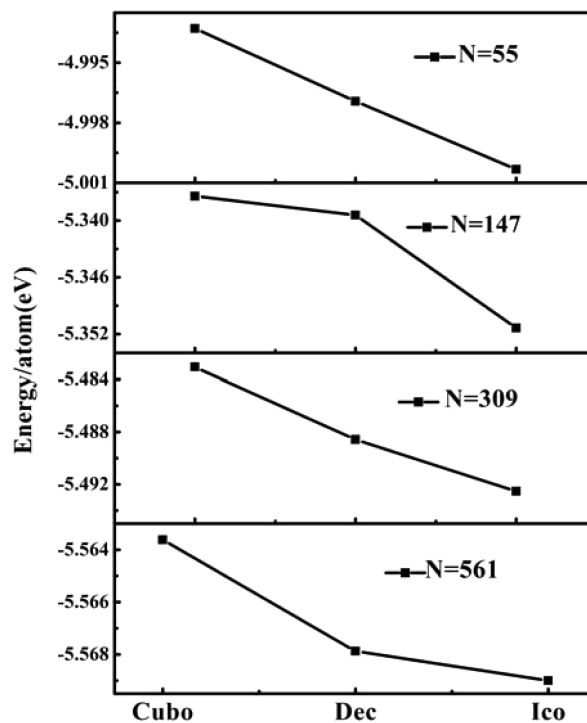


Figure 2. Plots of the total energy per atom of the CJ-structured Pd–Pt nanoalloys changing with the different cluster sizes (55, 147, 309, and 561) and morphologies (Cubo, Dec, and Ico).

where E is the potential energy, k_B is the Boltzmann constant, n is the total number of the atoms in the cluster, and T is the temperature.

Figure 3 shows the caloric curves and the heat capacities C_v per atom of CJ-structured Pd–Pt nanoalloys changing with the different cluster sizes (55, 147, 309, and 561) and morphologies (Cubo, Dec, and Ico). The temperature corresponding to the maximum peak value in the heat capacity C_v is in good agreement with the sharp jump in the caloric curve, which can be used to predict the melting temperature. On the basis of the position of the maximum peak value in the heat capacity C_v and the sharp jump in the caloric curve, the melting points of CJ-structured Pd–Pt nanoalloys changing with the different cluster sizes (55, 147, 309, and 561) and morphologies (Cubo, Dec, and Ico) can be estimated, as listed in Table 2.

Interestingly, the melting points of CJ-structured Pd–Pt nanoalloys with the same size follow the order of Ico > Dec > Cubo, which is in good agreement with the values of the stability of these nanoalloys (see Figure 2 and Table 2). This observation agrees with the rule that the more stable the cluster, the higher the melting point. Among these nanoalloys with the same size, the Ico structure is of the lowest value of the total energy per atom and also the highest melting point.

In order to understand the size effect on the melting properties of CJ-structured Pd–Pt nanoalloys, we identified the melting temperatures of these nanoalloys with different sizes. Figure 4 shows the melting temperatures of CJ-structured Pd–Pt nanoalloys with different morphologies (Cubo, Dec, and Ico) as a function of $N^{-1/3}$, where N represents the total number of clusters. Linear decrease in cluster melting point with $N^{-1/3}$ is found for CJ-structured Pd–Pt nanoalloys with the same morphology. It means that the melting temperature of CJ-structured Pd–Pt nanoalloys with the same morphology is

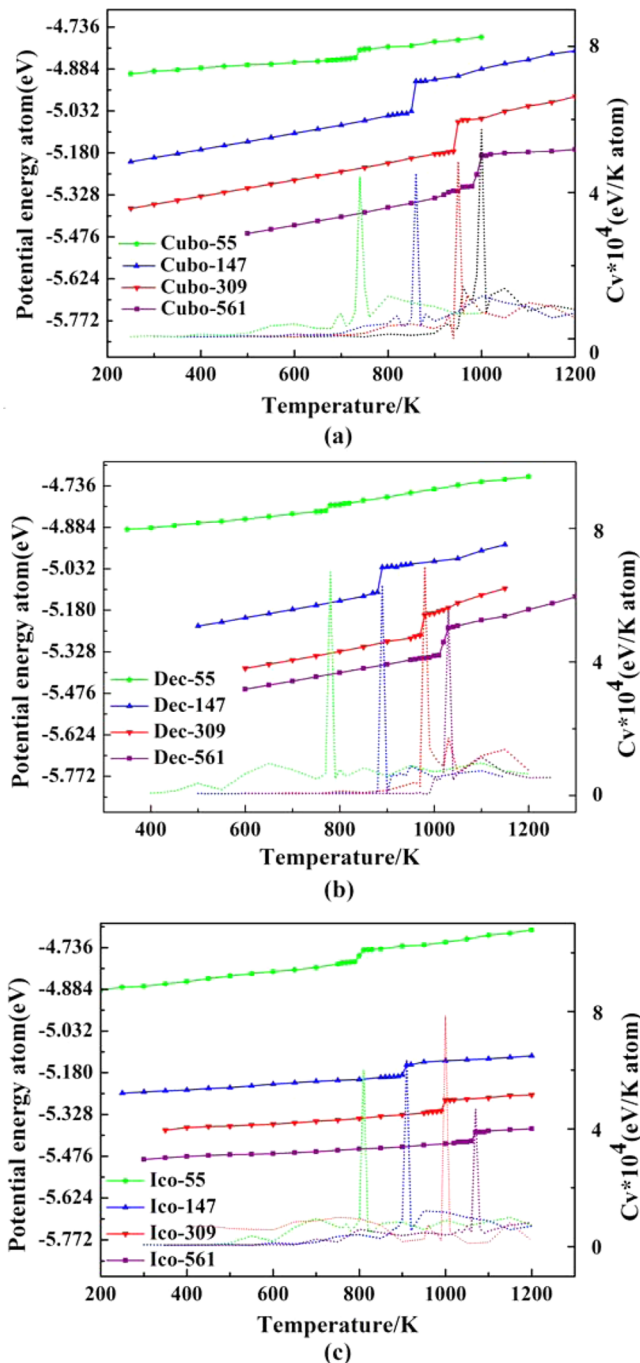


Figure 3. Caloric curves and the heat capacities C_v per atom of the CJ-structured Pd–Pt nanoalloys changing with the different cluster sizes (55, 147, 309, and 561) and morphologies (Cubo, Dec, and Ico).

Table 2. Melting Points of the CJ-Structured Pd–Pt Nanoalloys with the Different Cluster Sizes (55, 147, 309, and 561) and Morphologies (Cubo, Dec, and Ico)

structure	melting point/K	structure	melting point/K	structure	melting point/K
Cubo-55	740	Dec-55	780	Ico-55	810
Cubo-147	860	Dec-147	890	Ico-147	910
Cubo-309	950	Dec-309	980	Ico-309	1000
Cubo-561	1000	Dec-561	1010	Ico-561	1070

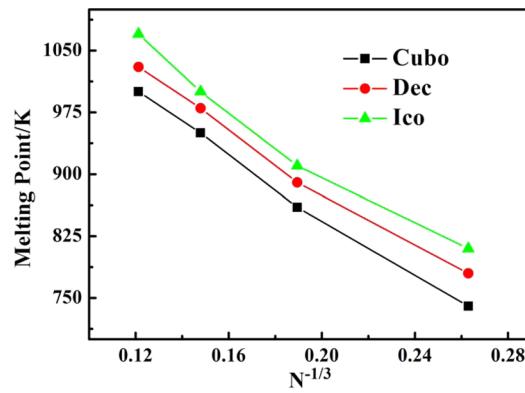


Figure 4. Melting temperatures of the CJ-structured Pd–Pt nanoalloys with different morphologies (Cubo, Dec, and Ico) as a function of $N^{-1/3}$, where N represents the total number of clusters.

of the same linear behavior as the inverse diameter of the clusters, which is in qualitative agreement with Pawlow's law.⁴⁴

3.3. Chemical Activity. In this work, the adsorption properties of O on these Pd–Pt nanoalloys are studied by using DFT calculations. For the CJ-structured $Pd_{12}Pt_{43}$, three morphologies were selected, corresponding to the highly symmetric Cubo, Dec, and Ico structures. For the CJ-structured $Pd_{12}Pt_{135}$, only the Ico structure was considered. In addition, the effect of O coverage was observed for the CJ-structured $Pd_{12}Pt_{43}$ with the Ico structure.

The nonequivalent adsorption sites for the CJ $Pd_{12}Pt_{43}$ with the Cubo, Dec, and Ico structures and $Pd_{12}Pt_{135}$ with the Ico structure are shown in Figure 5. For a Cubo structure with 55 atoms, nine nonequivalent adsorption sites are found, T1, T2, T3, B1, B2, B3, H1, H2, and H3, as shown in Figure 5a,b. For a Dec structure with 55 atoms, 18 possible adsorption sites can be found, T1–6, B1–8, and H1–4, as shown in Figure 5c,d. For an Ico structure with 55 atoms, 6 different adsorption sites are found, T1, T2, B1, B2, H1, and H2 sites, as shown in Figure 5e,f. Accordingly, 9 nonequivalent adsorption sites can be found for an Ico structure with 147 atoms (see Figure 5g,h).

The adsorption energy of O (E_{ads}) on these Pd–Pt nanoalloys at different adsorption sites is calculated by

$$E_{ads} = E_{cluster+nO} - E_{cluster} - nE_O \quad (5)$$

where $E_{cluster+nO}$ is the total energy of the cluster upon O absorption, $E_{cluster}$ is the energy of the free cluster, E_O is the energy of an isolated O in vacuum, and n is the number of O atoms.

The initial and final adsorption sites, adsorption energies, and metal–O bond lengths for the O absorption on the CJ $Pd_{12}Pt_{43}$ with the Cubo, Dec, and Ico structures and $Pd_{12}Pt_{135}$ with the Ico structure at all of the possible adsorption sites are calculated, as listed in Table S1 (Supporting Information).

3.3.1. Morphology Effect. The most favorable adsorption energies of the CJ-structured $Pd_{12}Pt_{43}$ with the Cubo, Dec, and Ico structures are listed in Table 3. It is found that the adsorption strength of O on the CJ-structured $Pd_{12}Pt_{43}$ follows the order of Dec < Cubo < Ico. Our results show that the CJ-structured $Pd_{12}Pt_{43}$ with the Dec structure exhibits the weakest O adsorption ability among these $Pd_{12}Pt_{43}$ clusters. It means that the Dec morphology could have superior catalysts performance, according to the rule that the weak O binding strength facilitates the ORR.

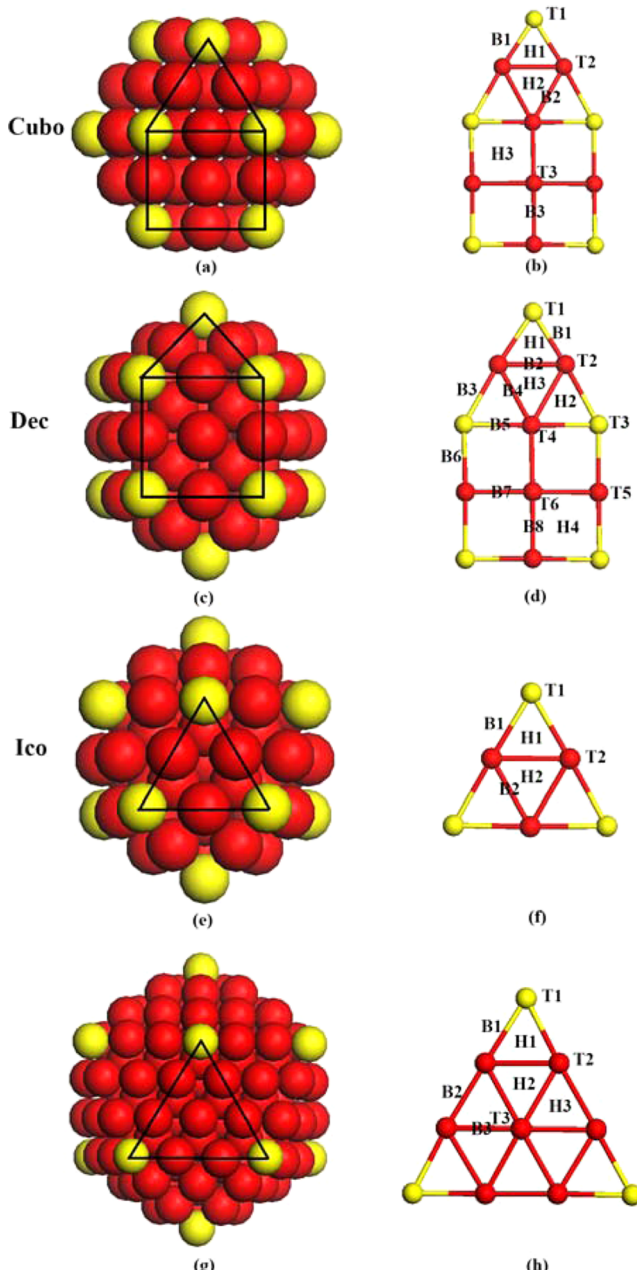


Figure 5. Optimized geometries and nonequivalent adsorption sites for the CJ-structured $\text{Pd}_{12}\text{Pt}_{43}$ with the Cubo (a,b), Dec (c,d), and Ico (e,f) structures and $\text{Pd}_{12}\text{Pt}_{135}$ with the Ico (g,h) structure. The Pd and Pt atoms are represented by yellow and rose spheres, respectively.

Table 3. Most Favorable Adsorption Energies of the CJ-Structured $\text{Pd}_{12}\text{Pt}_{43}$ with the Cubo, Dec, and Ico Structures and $\text{Pd}_{12}\text{Pt}_{135}$ with the Ico Structure

composition	Cubo	Dec	Ico
$\text{Pd}_{12}\text{Pt}_{43}$	-4.865	-4.751	-5.078
$\text{Pd}_{12}\text{Pt}_{135}$			-4.443

In order to understand the morphology effect on the O adsorption properties, the charge density difference for the CJ-structured $\text{Pd}_{12}\text{Pt}_{43}$ with the Cubo, Dec, and Ico structures upon O adsorption at the most favorable adsorption sites was calculated, as shown in Figure 6. It is found that the electrons of the O atom accumulate and metal atoms donate electrons. In

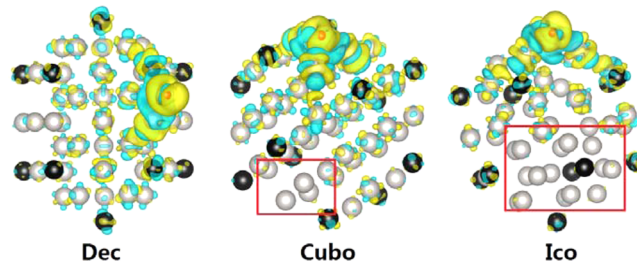


Figure 6. Charge density difference for the CJ-structured $\text{Pd}_{12}\text{Pt}_{43}$ with the Cubo, Dec, and Ico structures upon O adsorption at the most favorable adsorption sites. The electron accumulation and depletion are represented by yellow and blue surfaces, respectively. The black, white, and red atoms stand for Pd, Pt, and O atoms, respectively.

addition, the dumbbell-shaped region near the Pt atoms is found, corresponding to the Pt d_z^2 atomic orbital. For the Dec structure, charge redistribution is found for almost every metal atom. For the Cubo structure, charge redistribution is found for most of the metal atoms. In contrast, charge redistribution is found for only a few metal atoms in the Ico structure. The different charge redistribution in the Cubo, Dec, and Ico structures upon O adsorption can be used to explain their different adsorption strength of O, which follows the order of Dec < Cubo < Ico.

We also calculated the d-band center of the CJ-structured $\text{Pd}_{12}\text{Pt}_{43}$ with the Cubo, Dec, and Ico structures. Figure 7 shows

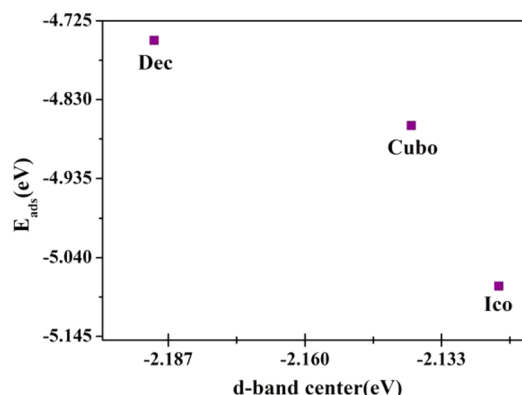


Figure 7. Adsorption energy (E_{ads}) of O at the most favorable adsorption sites versus the d-band center of the CJ-structured $\text{Pd}_{12}\text{Pt}_{43}$ with the Cubo, Dec, and Ico structures.

the adsorption energy of O at the most favorable adsorption sites versus the d-band center of the CJ-structured $\text{Pd}_{12}\text{Pt}_{43}$ with the Cubo, Dec, and Ico structures. It is found that the Dec structure possesses the most negative value of the d-band center and the weakest O adsorption strength among these morphologies. Our results show that the more negative the d-band center, the weaker the adsorption strength of O, which is in qualitative agreement with the previous DFT results.⁴⁵

3.3.2. Size Effect. The most favorable adsorption energies of the CJ-structured $\text{Pd}_{12}\text{Pt}_{43}$ and $\text{Pd}_{12}\text{Pt}_{135}$ with the Ico structure are listed in Table 3. It is found that the CJ-structured $\text{Pd}_{12}\text{Pt}_{43}$ is of stronger adsorption energy than the CJ-structured $\text{Pd}_{12}\text{Pt}_{135}$, indicating that the size can be used to modify the adsorption properties of the CJ-structured Pd–Pt nanoalloys. As listed in Table S1 (Supporting Information), the distance of the O and metal atoms ranges from 1.8 to 2.1 Å.

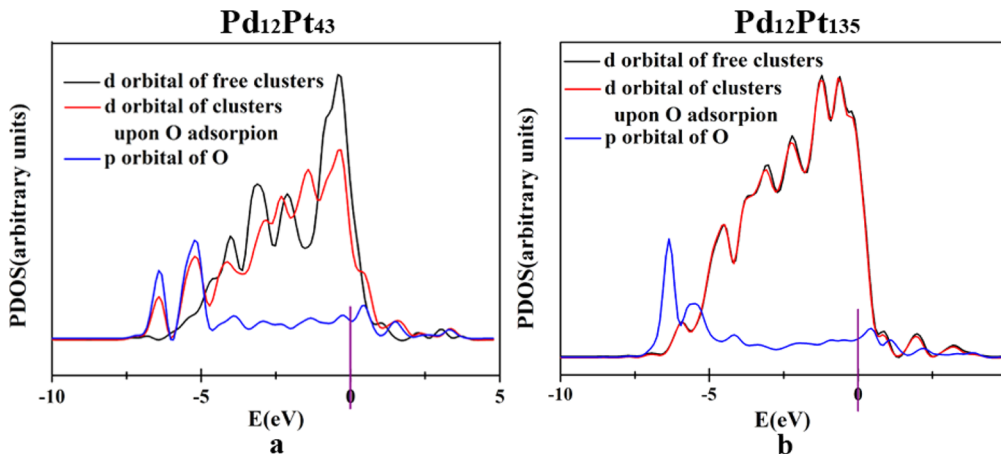


Figure 8. PDOSs of metal atoms close to the adsorbed O (d orbital) and O (p orbital) atom for the CJ-structured $\text{Pd}_{12}\text{Pt}_{43}$ and $\text{Pd}_{12}\text{Pt}_{135}$ with the Ico structure and upon O adsorption at the most favorable adsorption sites. The purple vertical line corresponds to the Fermi energy.

To explore the reason for the size effect on the O adsorption properties, we calculated the projected density of states (PDOS) of metal atoms close to the adsorbed O (d orbital) and O (p orbital) atom for the CJ-structured $\text{Pd}_{12}\text{Pt}_{43}$ and $\text{Pd}_{12}\text{Pt}_{135}$ with the Ico structure before and upon O adsorption at the most favorable adsorption sites, as shown in Figure 8. It is found that the d-PDOSs of the metal atoms change significantly upon O adsorption for the $\text{Pd}_{12}\text{Pt}_{43}$ cluster. In contrast, little change is observed in the d-PDOSs of the metal atoms upon O adsorption for the $\text{Pd}_{12}\text{Pt}_{135}$ cluster. This phenomenon can be used to explain the different adsorption strength of O on CJ-structured $\text{Pd}_{12}\text{Pt}_{43}$ and $\text{Pd}_{12}\text{Pt}_{135}$ with the Ico structure, which follows the order of $\text{Pd}_{12}\text{Pt}_{135} < \text{Pd}_{12}\text{Pt}_{43}$. In addition, the mixing between the d-PDOS of the metal atoms and the DOS (p orbital) of the O atom is found for the $\text{Pd}_{12}\text{Pt}_{43}$ cluster upon O adsorption, making a contribution to the formation of the strong metal–O bond, which is not significant for the $\text{Pd}_{12}\text{Pt}_{135}$ cluster upon O adsorption.

3.3.3. Coverage Effect. In order to understand the effect of the coverage of O on the O adsorption properties of the nanoalloys, we calculated the adsorption of O with 1, 5, 10, and 20 CJ-structured $\text{Pd}_{12}\text{Pt}_{43}$'s with the Ico structure at the H1 hollow site. Table 4 shows the adsorption energies per O atom

Table 4. Adsorption Energy of Icosahedral Clusters with Coverage (1O, 5O, 10O, 20O)

coverage	1O	5O	10O	20O
adsorption energy	-4.78	-4.60	-4.59	-4.58

for the adsorption of O on the H1 site of the CJ-structured $\text{Pd}_{12}\text{Pt}_{43}$ with the Ico structure with the number of O's increasing. It is found that the adsorption strength per O atom decreases slightly with increasing coverage of O atom on the CJ-structured $\text{Pd}_{12}\text{Pt}_{43}$.

Figure S1 (Supporting Information) shows the charge density difference of the adsorption of one and five O's on the H1 site of the CJ-structured $\text{Pd}_{12}\text{Pt}_{43}$. It is found that the charge transfer from the O to the metal atom for the case of five O's is much less than the case of one O. It means that the electrons of the bond between the O atom and metal atoms decrease when the number of O's increases from one to five, which weakens the adsorption strength per O atom.

4. CONCLUSIONS

We used Monte Carlo simulations, MD simulations, and DFT calculations to investigate the equilibrium structures, thermal stability, and chemical activity of crown-jewel (CJ)-structured Pd–Pt nanoalloys with highly symmetric cuboctahedral (Cubo), decahedral (Dec), and icosahedral (Ico) structures. For these Pd–Pt nanoalloys, all vertices of the cluster are occupied by 12 Pd atoms, corresponding to the typical CJ structure. It is found that the stability of CJ-structured Pd–Pt nanoalloys with the same size follows the order of Ico > Dec > Cubo. Interestingly, the melting points of CJ-structured Pd–Pt nanoalloys with the same size follow the order of Ico > Dec > Cubo, which is in good agreement with the order of the stability of these nanoalloys. This observation agrees with the rule that the more stable the cluster, the higher the melting point. In addition, the melting temperature of CJ-structured Pd–Pt nanoalloys with the same morphology is of the same linear behavior with the inverse diameter of the clusters, which is in qualitative agreement with Pawlow's law.

To investigate the chemical activity of these nanoalloys, the effects of the morphology, the size, and the coverage of O atoms on the adsorption properties of O on these Pd–Pt nanoalloys are studied. It is found that the adsorption strength of O on the CJ-structured $\text{Pd}_{12}\text{Pt}_{43}$ follows the order of Dec < Cubo < Ico. It is also found that the CJ-structured $\text{Pd}_{12}\text{Pt}_{43}$ is of stronger adsorption energy than the CJ-structured $\text{Pd}_{12}\text{Pt}_{135}$. In addition, the adsorption strength per O atom decreases slightly with increasing coverage of the O atom on the CJ-structured $\text{Pd}_{12}\text{Pt}_{43}$. Our results suggest that the structures, thermal stability, and chemical activity of CJ-structured Pd–Pt nanoalloys can be tuned by the size and morphology, which could provide useful insights for the design and development of CJ-structured nanoalloys as catalysts.

■ ASSOCIATED CONTENT

S Supporting Information

Table S1, giving the initial and final adsorption sites, adsorption energies, and metal–O bond lengths, and Figure S1, showing the charge density difference of the adsorption of O. This material is available free of charge via the Internet at <http://pubs.acs.org>.

AUTHOR INFORMATION

Corresponding Author

*E-mail: chengdj@mail.buct.edu.cn.

Notes

The authors declare no competing financial interest.

ACKNOWLEDGMENTS

This work is supported by the National Natural Science Foundation of China (21106003, 91334203), Beijing Higher Education Young Elite Teacher Project, Beijing Novel Program (Z12111000250000), “Chemical Grid Project” of BUCT, and Supercomputing Center of Chinese Academy of Sciences (SCCAS).

REFERENCES

- (1) Ferrando, R.; Johnston, R. Nanoalloys: From Theory to Applications of Alloy Clusters and Nanoparticles. *Chem. Rev.* **2008**, *108*, 845–910.
- (2) Liu, X.; Wang, D.; Li, Y. Synthesis and Catalytic Properties of Bimetallic Nanomaterials with Various Architectures. *Nano Today* **2012**, *7*, 448–466.
- (3) Wang, D.; Xin, H.; Yu, Y.; Wang, H.; Rus, E.; Muller, D. A.; Abruna, H. D. Pt-Decorated PdCo@Pd/C Core–Shell Nanoparticles with Enhanced Stability and Electrocatalytic Activity for the Oxygen Reduction Reaction. *J. Am. Chem. Soc.* **2010**, *132*, 17664–17666.
- (4) Di Noto, V.; Negro, E. Pt–Fe and Pt–Ni Carbon Nitride-Based ‘Core–Shell’ ORR Electrocatalysts for Polymer Electrolyte Membrane Fuel Cells. *Fuel Cells* **2010**, *10*, 234–244.
- (5) Chen, Y.; Yang, F.; Dai, Y.; Wang, W.; Chen, S. Ni@Pt Core–Shell Nanoparticles: Synthesis, Structural and Electrochemical Properties. *J. Phys. Chem. C* **2008**, *112*, 1645–1649.
- (6) Ferrer, D.; Torres-Castro, A.; Gao, X.; Sepulveda Guzman, S.; Ortiz Mendez, U.; Jose Yacaman, M. Three-Layer Core/Shell Structure in Au/Pd Bimetallic Nanoparticles. *Nano Lett.* **2007**, *7*, 1701–1705.
- (7) Baletto, F.; Mottet, C.; Ferrando, R. Growth of Three-Shell Onionlike Bimetallic Nanoparticles. *Phys. Rev. Lett.* **2003**, *90*, 135504.
- (8) Cheng, D.; Wang, W.; Huang, S.; Cao, D. Atomistic Modeling of Multishell Onion-Ring Bimetallic Nanowires and Clusters. *J. Phys. Chem. C* **2008**, *112*, 4855–4860.
- (9) Cheng, D.; Wang, W.; Huang, S. The Onion-Ring Structure for Pd–Pt Bimetallic Clusters. *J. Phys. Chem. B* **2006**, *110*, 16193–16196.
- (10) Zhang, H.; Watanabe, T.; Okumura, M.; Haruta, M.; Toshima, N. Catalytically Highly Active Top Gold Atom on Palladium Nanocluster. *Nat. Mater.* **2012**, *11*, 49–52.
- (11) Li, M.; Cheng, D. Molecular Dynamics Simulation of the Melting Behavior of Crown-Jewel Structured Au–Pd Nanoalloys. *J. Phys. Chem. C* **2013**, *117*, 18746–18751.
- (12) Gasteiger, H.; Kocha, S.; Sompalli, B.; Wagner, F. Activity Benchmarks and Requirements for Pt, Pt-Alloy, and Non-Pt Oxygen Reduction Catalysts for PEMFCs. *Appl. Catal., B* **2005**, *56*, 9–35.
- (13) Stamenkovic, V.; Fowler, B.; Mun, B.; Wang, G.; Ross, P.; Lucas, C.; Marković, N. Improved Oxygen Reduction Activity on Pt₃Ni (111) via Increased Surface Site Availability. *Science* **2007**, *315*, 493–497.
- (14) Chen, S.; Sheng, W.; Yabuuchi, N.; Ferreira, P.; Allard, L.; Shao Horn, Y. Origin of Oxygen Reduction Reaction Activity on ‘Pt₃Co’ Nanoparticles: Atomically Resolved Chemical Compositions and Structures. *J. Phys. Chem. C* **2008**, *113*, 1109–1125.
- (15) Koh, S.; Toney, M.; Strasser, P. Activity–Stability Relationships of Ordered and Disordered Alloy Phases of Pt₃Co Electrocatalysts for the Oxygen Reduction Reaction (ORR). *Electrochim. Acta* **2007**, *52*, 2765–2774.
- (16) Huang, Y.; Chou, T.; Yu, G.; Lee, S. Theoretical Study of Local Electronic Alloy Effects of OOH, OH, and O Adsorption on Pt–Pd Cluster Model. *J. Phys. Chem. C* **2011**, *115*, 9105–9116.
- (17) Lim, B.; Jiang, M.; Camargo, P.; Cho, E.; Tao, J.; Lu, X.; Zhu, Y.; Xia, Y. Pd–Pt Bimetallic Nanodendrites with High Activity for Oxygen Reduction. *Science* **2009**, *324*, 1302–1305.
- (18) Zhang, J.; Mo, Y.; Vukmirovic, M.; Klie, R.; Sasaki, K.; Adzic, R. Platinum Monolayer Electrocatalysts for O₂ Reduction: Pt Monolayer on Pd(111) and on Carbon-Supported Pd Nanoparticles. *J. Phys. Chem. B* **2004**, *108*, 10955–10964.
- (19) Tritsaris, G.; Greeley, J.; Rossmeisl, J.; Norskov, J. Atomic-Scale Modeling of Particle Size Effects for the Oxygen Reduction Reaction on Pt. *Catal. Lett.* **2011**, *1*–5.
- (20) Cheng, D.; Wang, W. Tailoring of Pd–Pt Bimetallic Clusters with High Stability for Oxygen Reduction Reaction. *Nanoscale* **2012**, *4*, 2408–2415.
- (21) Calvo, F. Solid-Solution Precursor to Melting in Onion-Ring Pd–Pt Nanoclusters: A Case of Second-Order-Like Phase Change? *Faraday Discuss.* **2008**, *138*, 75–88.
- (22) Cheng, D.; Huang, S.; Wang, W. Thermal Behavior of Core–Shell and Three-Shell Layered Clusters: Melting of Cu₁Au₅₄ and Cu₁₂Au₄₃. *Phys. Rev. B* **2006**, *74*, 064117.
- (23) Cheng, D.; Cao, D. Structural Transition and Melting of Onion-Ring Pd–Pt Bimetallic Clusters. *Chem. Phys. Lett.* **2008**, *461*, 71–76.
- (24) Claire, M.; Thomas, V.; Mortimer, J.; Roy, L. Geometries and Segregation Properties of Platinum–Palladium Nanoalloy Clusters. *J. Chem. Soc., Dalton Trans.* **2002**, *23*, 4375–4388.
- (25) Cleri, F.; Rosato, V. Tight-Binding Potentials for Transition Metals and Alloys. *Phys. Rev. B* **1993**, *48*, 22–33.
- (26) Cheng, D.; Wang, W.; Huang, S. Melting Phenomena: Effect of Composition for 55-Atom Ag–Pd Bimetallic Clusters. *Phys. Chem. Chem. Phys.* **2008**, *10*, 2513–2518.
- (27) Cheng, D.; Wang, W.; Huang, S. Thermal Evolution of Pd and Pd–Pt Clusters Supported on MgO(100). *J. Phys. Chem. C* **2007**, *111*, 8037–8042.
- (28) Cheng, D.; Yuan, S.; Ferrando, R. Structure, Chemical Ordering and Thermal Stability of Pt–Ni Alloy Nanoclusters. *J. Phys.: Condens. Mater.* **2013**, *25*, 355008.
- (29) Paz Borbon, L.; Johnston, R.; Barcaro, G.; Fortunelli, A. Structural Motifs, Mixing, and Segregation Effects in 38-Atom Binary Clusters. *J. Chem. Phys.* **2008**, *128*, 134517.
- (30) Sankaranarayanan, S.; Bhethanabotla, V.; Joseph, B. Molecular Dynamics Simulation Study of the Melting of Pd–Pt Nanoclusters. *Phys. Rev. B* **2005**, *71*, 195415.
- (31) Mottet, C.; Rossi, G.; Baletto, F.; Ferrando, R. Single Impurity Effect on the Melting of Nanoclusters. *Phys. Rev. Lett.* **2005**, *95*, 035501.
- (32) Kuntová, Z.; Rossi, G.; Ferrando, R. Melting of Core–Shell Ag–Ni and Ag–Co Nanoclusters Studied via Molecular Dynamics Simulations. *Phys. Rev. B* **2008**, *77*, 205431.
- (33) Oderji, H.; Behnejad, Ferrando, H.; Riccardo, Ding, H. System-Dependent Melting Behavior of Icosahedral Anti-Mackay Nanoalloys. *RSC Adv.* **2013**, *3*, 21981–21993.
- (34) Giannozzi, P.; Baroni, S.; Bonini, N.; Calandra, M.; Car, R.; Cavazzoni, C.; Ceresoli, D.; Chiarotti, G. L.; Cococcioni, M.; Dabo, I. Quantum Espresso: A Modular and Open-Source Software Project for Quantum Simulations of Materials. *J. Phys.: Condens. Matter* **2009**, *21*, 395502.
- (35) Perdew, J. P.; Burke, K.; Ernzerhof, M. Generalized Gradient Approximation Made Simple. *Phys. Rev. Lett.* **1996**, *77*, 3865–3868.
- (36) Vanderbilt, D. Soft Self-Consistent Pseudopotentials in a Generalized Eigenvalue Formalism. *Phys. Rev. B* **1990**, *41*, 7892–7895.
- (37) Methfessel, M.; Paxton, A. High-Precision Sampling for Brillouin-Zone Integration in Metals. *Phys. Rev. B* **1989**, *40*, 3616–3621.
- (38) Aprà, E.; Baletto, F.; Ferrando, R.; Fortunelli, A. Amorphization Mechanism of Icosahedral Metal Nanoclusters. *Phys. Rev. Lett.* **2004**, *93*, 065502.
- (39) Baletto, F.; Ferrando, R.; Fortunelli, A.; Montalenti, F.; Mottet, C. Crossover among Structural Motifs in Transition and Noble-Metal Clusters. *J. Chem. Phys.* **2002**, *116*, 3856–3863.

- (40) Qi, Y.; Çağın, T.; Kimura, Y.; Goddard, W. A., III. Molecular-Dynamics Simulations of Glass Formation and Crystallization in Binary Liquid Metals: Cu–Ag and Cu–Ni. *Phys. Rev. B* **1999**, *59*, 3527–3533.
- (41) Wen, Y.; Zhang, Y.; Zheng, J.; Zhu, Z.; Sun, S. Orientation-Dependent Structural Transition and Melting of Au Nanowires. *J. Phys. Chem. C* **2009**, *113*, 20611–20617.
- (42) Ikeda, H.; Qi, Y.; Cagin, T.; Samwer, K.; Johnson, W.; Goddard, W. A., III. Strain Rate Induced Amorphization in Metallic Nanowires. *Phys. Rev. Lett.* **1999**, *82*, 2900–2903.
- (43) Huang, R.; Wen, Y.; Zhu, Z.; Sun, S. Thermal Stability of Platinum Nanowires: A Comparison Study between Single-Crystalline and Twinned Structures. *J. Mater. Chem.* **2011**, *21*, 18998–19004.
- (44) Pawlow, P. Über Die Abhängigkeit Des Schmelzpunktes von der Oberflächenenergie Eines Festen Körpers. *Z. Phys. Chem.* **1909**, *6S*, 1–35.
- (45) Xu, W.; Cheng, D.; Niu, M.; Shao, X.; Wang, W. Modification of the Adsorption Properties of O and OH on Pt–Ni Bimetallic Surfaces by Subsurface Alloying. *Electrochim. Acta* **2012**, *76*, 440–445.